Cell, Vol. 102, 809–816, September 15, 2000, Copyright ©2000 by Cell Press

The 4 Å X-Ray Structure of a Tubulin:Stathmin-like Domain Complex

Benoît Gigant,*‖ Patrick A. Curmi,†‖ Carole Martin-Barbey,*‖ Elodie Charbaut,† Sylvie Lachkar,† Luc Lebeau,‡ Samila Siavoshian,*† André Sobel,† and Marcel Knossow*§

*Laboratoire d'Enzymologie et Biochimie Structurales
C.N.R.S. U.P.R. 9063
1 avenue de la Terrasse
91198 Gif sur Yvette Cedex
France

†INSERM U 440
Institut du Fer à Moulin
17 rue du Fer à Moulin
75005 Paris
France

‡C.N.R.S. UMR 7514
Faculté de Pharmacie
67401 Illkirch Cedex
France

Summary

Phosphoproteins of the stathmin family interact with the αβ tubulin heterodimer (tubulin) and hence interfere with microtubule dynamics. The structure of the complex of GDP-tubulin with the stathmin-like domain of the neural protein RB3 reveals a head-to-tail assembly of two tubulins with a 91-residue RB3 α helix in which each copy of an internal duplicated sequence interacts with a different tubulin. As a result of the relative orientations adopted by tubulins and by their α and β subunits, the tubulin:RB3 complex forms a curved structure. The RB3 helix thus most likely prevents incorporation of tubulin into microtubules by holding it in an assembly with a curvature very similar to that of the depolymerization products of microtubules.

Introduction

Stathmin (Sobel et al., 1989), also referred to as Op 18 (Hailat et al., 1990), is a 17 kDa ubiquitous cytosolic phosphoprotein that has been proposed to be a relay integrating diverse intracellular signaling pathways (Sobel, 1991). Stathmin has recently been recognized as a microtubule destabilizing factor (Belmont and Mitchison, 1996) likely to be implicated in various microtubule-dependent cellular functions in interphase or mitosis (Marklund et al., 1996; Di Paolo et al., 1997; Horwitz et al., 1997; Gavet et al., 1998). Stathmin influences microtubule dynamics in vitro and in vivo either by preventing assembly or promoting disassembly of microtubules in a concentration-dependent manner. These effects on microtubules are abolished or dramatically reduced by its phosphorylation by kinases or by mutations that mimic phosphorylation (Di Paolo et al., 1997; Horwitz et al., 1997; Melander Gradin et al., 1997; Gavet et al., 1998; Gradin et al., 1998). Molecular delineation of the microtubule destabilization activity of stathmin showed that it hinges on the necessary presence of an 84-residue core that must be extended either on its N or C side to be active, the shortest stathmin active region identified so far comprising 95 residues (Redeker et al., 2000). Stathmin is also the generic element of a protein family which includes the neural proteins SCG10, RB3, and SCLIP (Ozon et al., 1997), that share a highly conserved stathmin-like domain (Maucuer et al., 1993; Ozon et al., 1997) and microtubule destabilization potential (Riederer et al., 1997; Antonsson et al., 1998; Gavet et al., 1998).

The mechanism by which stathmin influences microtubule dynamics is still a matter of debate as various stathmin activities have been reported. We found in vitro that the effects of stathmin can be inferred from its ability to form a ternary complex sequestering free tubulin (in what follows the tubulin polypeptide chains are designated as the α and β tubulin subunits and the αβ heterodimer as tubulin). This complex comprises two tubulins and one stathmin (Curmi et al., 1997; Jourdain et al., 1997) as also recently found by others (Larsson et al., 1999; Steinmetz et al., 2000). Alternatively, it has also been proposed that stathmin could directly increase the frequency of microtubule catastrophes (Belmont and Mitchison, 1996), an effect possibly triggered by an interaction with microtubule ends (Howell et al., 1999; Steinmetz et al., 2000).

Formation of the tubulin:stathmin complex presented a new way to stabilize tubulin in solution for crystallization. Many attempts have been made to characterize structurally this protein which exists in three major forms: microtubules, heterodimers, and curved oligomers. Difficulty in producing three-dimensional tubulin crystals has been attributed to (1) the heterogeneity of tubulin preparations caused by posttranslational modifications of tubulin isoforms, (2) the instability of tubulin in solution, and (3) the heterodisperse nature of tubulin preparations. The only near-atomic resolution structure of tubulin was derived from a 3.7 Å electron density map obtained by electron crystallography (Nogales et al., 1998); it is that of tubulin in protofilaments arranged in an antiparallel way in two-dimensional zinc-induced sheets. In addition, the overall shape of the tubulin:stathmin complex has been suggested by scanning transmission electron microscopy combined with digital image processing to be that of a kinked protofilament-like assembly of two tubulins (Steinmetz et al., 2000). At the nominal 2 nm resolution of the planar projection electron micrographs, neither the ordering of tubulins in the complex nor the localization of stathmin could be defined.

We report here the 4 Å X-ray structure of a complex of GDP-tubulin with the *Escherichia coli* expressed stathmin-like domain of RB3 (RB3-SLD), a stathmin family protein. This structure defines the 3D shape of the complex, the arrangement of tubulins within this complex, and shows that RB3 extensively contacts tubulin through a 91-residue α helix. The results provide a clear

§To whom correspondence should be addressed (e-mail: knossow@lebs.cnrs-gif.fr).

‖These authors contributed equally to this work.

Table 1. Crystallographic Data and Refinement Statistics

Data Collection Statistics	
Space group P65, a (= b) = 328.5 Å, c = 54.4 Å	
Resolution	50–3.95 Å
Unique Reflections	29,784
Completeness (%)[a]	99.1 (98.7)
Completeness (F > 0σ) (%)[a]	95.8 (89.5)
Redundancy[a]	4.1 (3.0)
Rsym[b] (%)[a]	6.2 (33.3)
I/σ(I)[a]	18.9 (2.9)
Refinement Statistics	
Resolution	7.0–3.95 Å
Completeness (F > 0 σ)	94.3%
R[c] (%)	27.2
R_{free} (%)	36.1
Mean B factor (all atoms) (Å)^2	86
Rms deviations from ideality	
Bond lengths (Å)	0.012
Bond angles (°)	1.84
Rms deviation ncs (Å)[d]	0.071
Sigmaa coordinate error (Å)	0.76

[a] The number in parentheses is the value in the 4.02–3.95 Å resolution shell.

[b] $R_{sym} = \Sigma\Sigma_j|I_j - \langle I\rangle|/\Sigma|\langle I\rangle|$ where I_j is the intensity measurement for reflection j and $\langle I\rangle$ is the mean intensity for multiply recorded reflections.

[c] $R = \Sigma||F_{obs}| - |F_{calc}||/\Sigma|F_{obs}|$ for all $F > 0\ \sigma$. R_{free} is calculated with 5% of the reflections not included in the refinement.

[d] Rmsd between the two tubulins of the T2R complex.

model for tubulin sequestration by stathmin family proteins and the tubulin:RB3-SLD complex (referred to as T2R) provides a structure of GDP-tubulin which is compared with the structure of tubulin in microtubules.

Results

Purification, Crystallization, and Structure Determination of the Tubulin:RB3-Stathmin-like Domain Complex

Crystallization trials by vapor diffusion (see Experimental Procedures) were set up using tubulin mixed in stoichiometric proportions with stathmin or stathmin-like domains (SLD) of the stathmin family, to yield 2:1 complexes. GDP-tubulin was used throughout crystallization trials, as we found that the apparent affinity of the GDP-tubulin:stathmin interaction, as defined by plasmon resonance technology, is 5 times higher than that of the GTP-tubulin:stathmin ($K_D = 0.2 \pm 0.03 \times 10^{-6}$ M for GDP-tubulin and $1 \pm 0.2 \times 10^{-6}$ M for GTP-tubulin). The best crystallization results were with RB3-SLD, which has the same respective apparent affinities for GDP-tubulin and GTP-tubulin as stathmin. Hexagonal crystals, space group $P6_5$ (a = b = 328.5 Å, c = 54.4 Å) were obtained. The crystals contain one 220 kDa T2R complex per asymmetric unit, with a solvent content of 68%. They are radiation sensitive; diffraction to a maximal resolution of 3.75 Å was observed with crystals maintained at 100 K and a complete diffraction data set was processed at 3.95 Å resolution ($R_{sym} = 0.062$, R_{sym} in the 4–3.95 Å resolution shell = 0.33, see Table 1). The tubulin moiety of the complex was localized by the Molecular Replacement method (Navaza, 1994). Rigid body refinement at 7 Å resolution showed that the correlation coefficients of observed and calculated structure factors after rigid-body refinement of the four Cα-only models of the polypeptide chains (0.57 in the 15–7 Å range) is significantly higher than after rigid-body refinement of two protofilament-like αβ dimers (0.43 in the same resolution range). Therefore, the final model resulting from the Molecular Replacement procedure consisted of two α and two β tubulin subunits (Nogales et al., 1998) refined as four separate rigid bodies using diffraction data to 3.95 Å; the corresponding correlation coefficient of observed and calculated structure factors was 0.51 in the 15–3.95 Å resolution range. There was no unfavorable steric interaction between tubulin subunits in the crystal.

Modeling and Refinement

The first cycles of refinement, constrained by the noncrystallographic symmetry relating the two tubulins, reduced the crystallographic R factor from 0.53 to 0.41; these were followed by density modification (Abrahams and Leslie, 1996), which resulted in a dramatically improved map where secondary structure and well-connected main chain density was seen over most of the two tubulins; this map revealed a long connected density lining the two tubulins, detached from any other density, where a kinked 91-residue polyAla helix partial RB3-SLD model could be built (Figure 1). After refinement of atomic positions and temperature factors the R factor is 0.27 for data in the 7–3.95 Å resolution range ($R_{free} = 0.36$). The model presented here contains about 90% of the main chain of tubulin and four nucleotides (2 GTP and 2 GDP molecules, see Experimental Procedures); most of the missing residues are in the C-terminal posttranslationally modified parts of the tubulin subunits and in a presumably disordered loop which connects helix H1 and strand S2 (definition of the secondary structure elements of tubulin subunits as in Nogales et al., 1998, 1999). The RB3-SLD long connected density has been modeled as a 91-residue polyAla α helix; 50 RB3-SLD residues are missing from our model.

The structure is consistent with biophysical data available in the literature (which was not used to guide our model-building). Available evidence supporting the model includes the following. (1) The RB3-SLD model is in keeping with the estimate of helical content of stathmin that was deduced from an analysis of the far UV circular dichroism to be in the 45%–60% range, which corresponds to 66–89 residues out of 149 (Curmi et al., 1994; Steinmetz et al., 2000). (2) The morphology of the T2R complex and its longest dimension and width (176 Å and 40 Å) are very similar to those deduced from averaged electron micrographs of the tubulin:stathmin complex, which had corresponding measured dimensions of 176 Å and 55 Å (Steinmetz et al., 2000). Moreover, the angle made by the two tubulins of the tubulin:stathmin complex (25 ± 4°) as deduced from electron micrographs (Steinmetz et al., 2000) is identical within the experimental error with the angle (27°) made by the lines joining the centers of the α and β subunits in each of the tubulins in T2R.

Tubulin αβ Heterodimers Arrange Head-to-Tail and Form an Extensive Interface with RB3-SLD

The T2R structure comprises one RB3-SLD together with a curved assembly of two tubulins arranged head-to-tail (Figure 1a), so that when numbering subunits sequentially from one end of the complex the order is

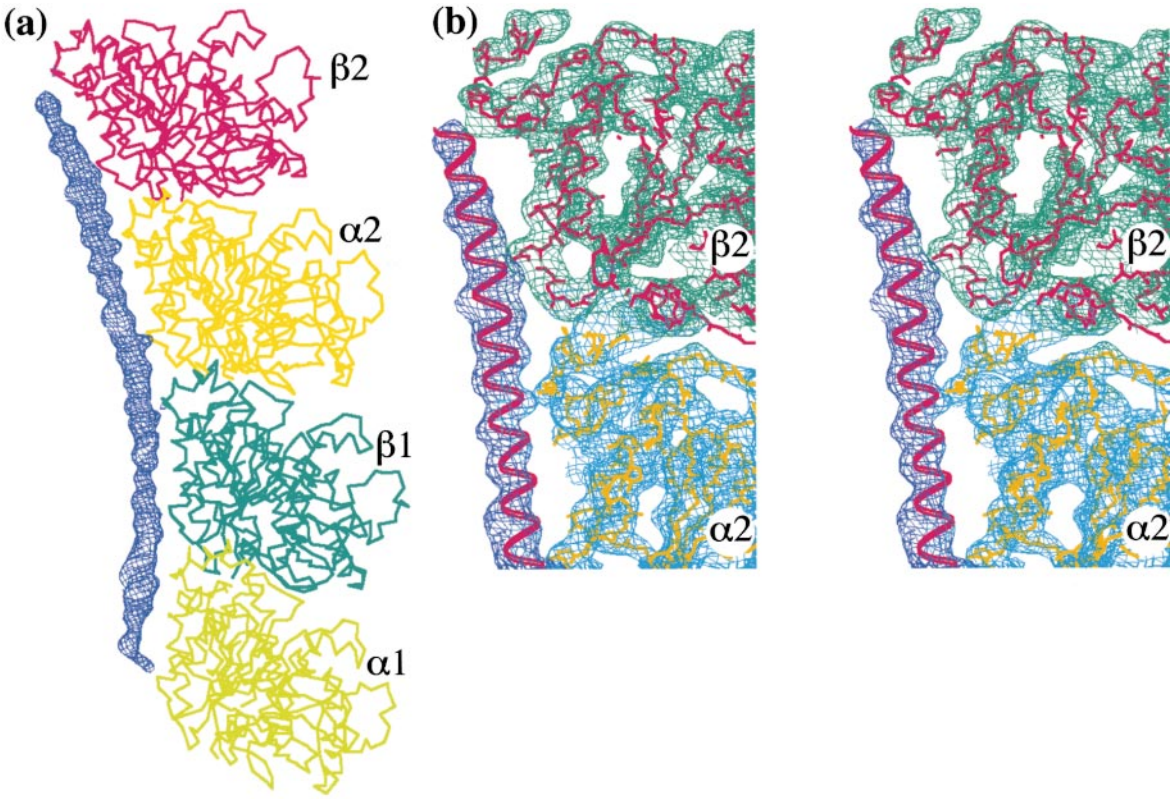

Figure 1. The T2R Electron Density Map

The Fourier synthesis map was calculated using phases from the tubulin model and density modification. (a) The long density stretch attributed to RB3-SLD (blue) is contoured at the 1 standard deviation level of the map. It is represented along the two tubulins used in the calculation of the structure factors (drawn as Cα traces). (b) Stereo close-up of the T2R electron density overlapped with the RB3-SLD α helix polyAla model. Figure 1 has been represented using the Bobscript program (Esnouf, 1997).

($\alpha_1\beta_1\alpha_2\beta_2$). A 91-residue long RB3-SLD α helix runs from one end of the tubulin assembly to the other making extensive contacts with it: 1280 Å^2 of the tubulin surface are buried by the polyAla model of the RB3-SLD α helix. The RB3-SLD α helix contacts mainly four regions of each tubulin subunit in the complex (Figure 2). Tubulin α and β subunits consist of three structural domains (Nogales et al., 1998); these are the nucleotide binding domain (residues 1 to 205), an intermediate domain (residues 206 to 384) and the C-terminal domain composed of two α helices (residues 385 to the C terminus). The four RB3-SLD contacting peptides belong to the N-terminal domain (three peptides) and to the C-terminal domain (one peptide); no contact is made to the intermediate domain by the RB3-SLD α helix. Most interestingly, the positions in the sequence of the residues contacted by the RB3 α helix are very similar in all four tubulin subunits.

As a consequence of the change of the relative orientations of tubulin subunits in T2R with respect to Zn sheet and straight microtubule protofilaments (see below), the buried areas at the interface between tubulin subunits are significantly smaller in T2R than in protofilaments ($\alpha_1\beta_1$: 2200 Å^2, $\beta_1\alpha_2$: 1960 Å^2 in T2R, as calculated in CCP4 [CCP4, 1994] compared to about 3000 Å^2 in straight microtubule protofilaments [Nogales et al., 1999]). Among the three zones of contact of tubulin subunits that have been identified (Nogales et al., 1999), only the one closest to RB3, involving interactions of the H8 helix with the T3, T5 and H11-H12 loops of the neighboring subunit, maintains contacts of similar extent in T2R and protofilaments (see Figure 2 for the location of secondary structure elements). Further from the RB3 helix, the H10 helix and H10-S9 loop and the H7-H8 loop (also referred to as the T7 loop; Nogales et al., 1999) make far less contacts in T2R than in the protofilament.

A 400 Å Pitch Helix Building Block

By contrast with the arrangement of tubulin in zinc sheets (Nogales et al., 1998) and with the straight protofilaments observed in microtubules by electron microscopy (Mandelkow et al., 1991), the T2R complex is curved (Figure 1). In RB3-SLD the T2R curvature is accommodated by a kinked α helix; it appears that the kink is located approximately in the middle of this helix. To provide a measure of the relative orientations of the tubulin subunits that yield the observed curvature, we determined the transformations that superimpose their nucleotide binding domains which are their structurally best conserved component (root mean square deviation [rmsd] of their Cαs after superposition: 1.4 Å). These transformations comprise a translation and a rotation; the rotation angles are a measure of the relative orientations of the tubulin subunits. These are: (α_1, β_1) = (α_2, β_2) = 11°, (β_1, α_2) = 13° and (α_1, β_2) = 34°. The (α_1, β_1) and (α_2, β_2) angles are much larger than the angle (close

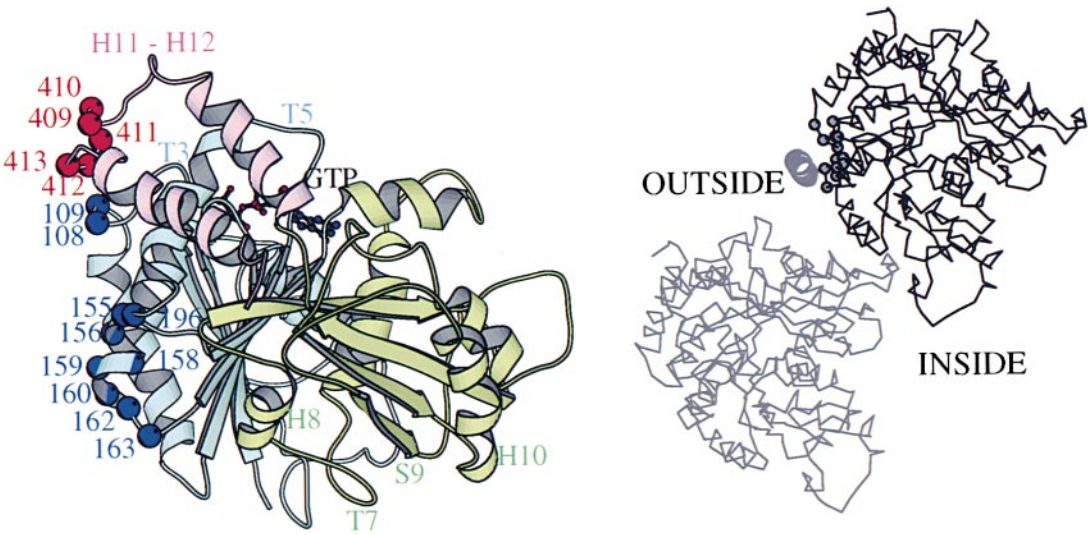

Figure 2. Positions of Tubulin Subunits Where Contacts Are Made with the RB3-SLD α Helix

Residues were considered to contact the RB3-SLD α helix when their Cαs were distant by less than 8 Å from Cαs of the RB3-SLD α helix; 15 positions in four different peptides were identified and at 10 of them contacts are made with the RB3-SLD α helix in each of the four tubulin subunits of T2R. All contacts are represented on the same tubulin α subunit. (Left) Footprint of the RB3-SLD on a tubulin subunit. The N-terminal nucleotide binding domain is in light blue, with its bound nucleotide drawn in ball-and-stick and residues contacting the RB3-SLD α helix highlighted as blue spheres. The second domain is in light green and the C-terminal domain is in pink. In the N-terminal domain the contacts with the RB3-SLD α helix are made by the end of the loop connecting strand S3 and helix H3 (residues 108 and 109), the two C-terminal turns of the H4 helix and the first residues of the H4–S5 turn (residues 155, 156, 158, 159, 162, and 163) and one residue in the H5–S6 turn (residue 196). In the C-terminal domain, the RB3-SLD α helix contacts the turn that precedes the H12 helix (residues 409 to 413, highlighted as red spheres). (Right) Modeled footprint of the RB3-SLD α helix on a straight protofilament in a microtubule (Nogales et al., 1999); the modeling is such that the RB3-SLD helix would interact with the same residues as it does in T2R. Two adjacent tubulin α subunits are drawn as Cα traces in this cross section of the microtubule. On one of these tubulin α subunits, residues contacting the RB3-SLD α helix in T2R are shown as spheres and the corresponding RB3-SLD moiety is represented as a helix ribbon. The shortest distance of the Cαs of this RB3-SLD region to the Cαs of the adjacent protofilament would be 14 Å. Atomic coordinates of two neighboring protofilaments in a microtubule were kindly provided by Dr. E. Nogales. Figures 2 and 3 have been drawn with Molscript (Kraulis, 1991).

to 0°) of the rotation that superimposes the nucleotide binding domains in the α and β subunits in a zinc sheet protofilament (Nogales et al., 1998). The overall curvature we observe is due both to a deformation of each tubulin and to the angle made by tubulins.

The 3D curvature of the complex is best pictured by building a $(T2R)_n$ superstructure resulting from the repetition of T2R (Figure 3). This yields a helical structure with a 400 Å pitch. The number of tubulins per turn (16) is identical to that in the outer ring of the double-ring polymerized tubulin (Diaz et al., 1994) and the radii are very similar (225 Å versus 210 Å). Thus, the conformation of tubulin in T2R is likely to be very similar to that of tubulin in GDP-tubulin oligomers, which form both rings and helical entities.

Discussion

The stathmin-like domain of RB3 and stathmin have a high degree of sequence similarity (Ozon et al., 1997) and similar biochemical properties, including identical apparent affinities for tubulin. In addition, comparison of electron micrographs of the tubulin:stathmin complex (Steinmetz et al., 2000) with the T2R structure suggests that the structures of the complexes of these two proteins with tubulin are similar. Taken together, the structural and biochemical data suggest that stathmin and RB3-SLD interact in the same way with tubulin. In what follows, we will interpret our data in the light of results from experiments on stathmin or on RB3-SLD.

Our model of the tubulin:RB3-SLD complex defines the length of the RB3-SLD α helix that interacts with tubulin. This length (91 residues) is in the upper range of those of the fragments predicted to be mostly α-helical by the algorithms applied to the sequence of stathmin (Doye et al., 1989; Maucuer et al., 1990; Redeker et al., 2000; Steinmetz et al., 2000). Among secondary structure prediction algorithms, PHDsec (Rost et al., 1994) predicts the longest α-helical region which in RB3-SLD extends from Ser46 to Ser107 and from Lys109 to Lys137 (RB3-SLD residue numbering is as defined in Experimental Procedures), i.e., a total length of 92 residues. Thermal denaturation studies show that the stathmin long α helix is marginally stable, being largely denatured at 40°C (Steinmetz et al., 2000; Wallon et al., 2000); complex formation with tubulin is thus likely to enhance the α helix content of RB3-SLD and/or to stabilize it.

Tubulin–Stathmin Interactions

Our model also identifies four peptides of each tubulin subunit involved in interactions with the RB3-SLD α helix. The corresponding residues are completely conserved in all α tubulin subunits and, as a different sequence, in all tubulin β subunits. Interestingly, most of the positions in the sequences of the α and β subunits where residues contact the RB3-SLD α helix are identical in the two tubulin αβ heterodimers of the complex. This conservation of the positions of tubulin amino acids that interact with the RB3-SLD α helix correlates with a sequence duplication in a region of the RB3 stathmin-like domain (residues 48 to 133, see Figure 4) that almost

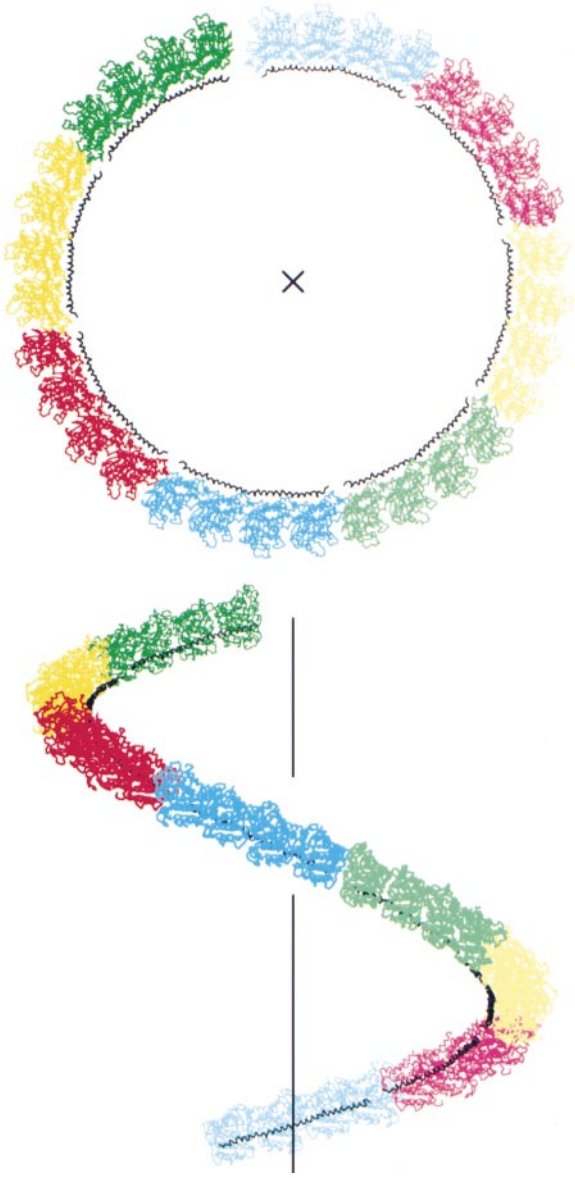

Figure 3. The $(T2R)_n$ Structure Resulting from the Repetition of T2R which Illustrates the Curvature of This Complex

This picture was obtained by superimposing the $\alpha_1\beta_1$ moiety of the m^{th} complex onto the $\alpha_2\beta_2$ moiety of the $(m-1)^{th}$ complex and by keeping in the final structure $(\alpha_1\beta_1)_1$, $(\alpha_2\beta_2)_1$, $(\alpha_2\beta_2)_2$,..., $(\alpha_2\beta_2)_n$. Each T2R complex, drawn as a Cα trace, is in a different color from its neighbors except the RB3-SLD helix which is in black. Top: view along the helix axis (noted as a cross); 8 complexes are represented. Bottom: view perpendicular to the helix axis, which is noted as a straight line; one turn of the helix, i.e., 8 T2R complexes, is represented.

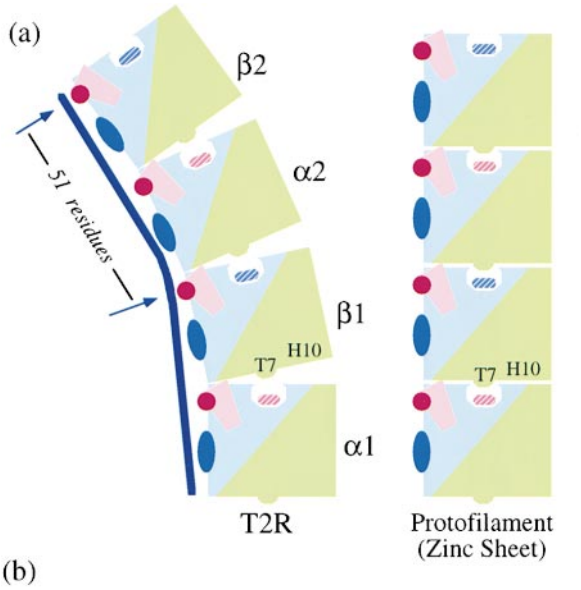

(b)

```
48 EEIQKKLEAAEERRKYQEAELLKHLAEKREHEREV 82
   E++ +K+E+ +E R+   A +L+ L EK +H  EV
99 EKLAQKMESNKENREAHLAAMLERLQEKDKHAEEV 133
```

Figure 4. Comparison of T2R and Zinc Sheet Protofilament Tubulin

(a) Schematic representation of the changes of the orientations of tubulin subunits in T2R as compared to straight protofilaments. The same colour code is used to identify tubulin subunits domains as in Figure 2. Nucleotides are represented as crosshatched blue (GDP) and red (GTP) motifs. T7 and H10 indicate the localizations of the T7 loop and of the H10 helix (intermediate domain, light green) that contact the neighboring subunit in Zn^{2+} sheet protofilaments (Nogales et al., 1999) (right) but not in T2R (left). The stathmin-like domain long α helix is represented by a thick dark blue line in T2R. The localizations of tubulin residues of the C-terminal domain and of the nucleotide binding domain that contact the stathmin-like domain long α helix are also noted (full circle and full oval, respectively). (b) Alignment of the RB3-SLD sequence with itself. The sequence alignment was performed with BLAST (Altschul et al., 1997), which detects 13 identities and 23 similarities over two 35-residue regions with a 16-residue gap. Only the regions of RB3-SLD with a significant sequence similarity are represented (top and bottom lines); identical residues and similarities (+) are plotted on the middle line. Residue numbering is as defined in Experimental Procedures. The sequence spacing of the stathmin-like domain residues with identical tubulin contacts is represented in (a) and corresponds to the spacing of the aligned stathmin-like domain residues.

coincides with that predicted to have a high helical propensity by the PHDsec algorithm (residues 46 to 137). Similarly to what has been found in stathmin (Maucuer et al., 1990), we identified a 35 amino acid duplication (37% sequence identity, 65% sequence similarity—alignment performed with BLAST; Altschul et al., 1997) with a 16 amino acid gap. Consistent with the spacing of the two copies of the duplicated sequence, the residues of the RB3-SLD α helix interacting with identical residues in the two tubulins of T2R are separated by 51 residues. Therefore, the region containing the duplicated peptide is likely to be included in the one we observe in T2R. Moreover, the equal spacing between corresponding residues in the duplicated peptides of RB3-SLD and between the residues of RB3-SLD that interact with identical residues of tubulin reinforces the notion that establishing a complex with tubulin is one of the major functions of the stathmin-like domains of stathmin family proteins.

Mechanisms for Regulation of Microtubule Assembly by Stathmin

The length and likely location in the RB3-SLD sequence (92 residues, positions 46–137) of the RB3-SLD helix that contacts tubulin are very similar to the length and location (95 residues, residues 44 to 138) of a proteolytic fragment of stathmin that binds tubulin and inhibits tubulin polymerization; in these assays, stathmin and this

95-residue fragment (F) have undistinguishable efficiencies (Redeker et al., 2000). Taken together with the curved structure of T2R, this suggests that a T2F complex where the RB3 fragment would be very similar to the long helix we identified cannot be incorporated into microtubules. The long RB3-SLD helix does not cap the plus or minus end of the tubulin moiety of T2R and there would be no steric hindrance with neighboring protofilaments of an RB3-SLD helix bound to one protofilament and interacting with the same tubulin residues as in T2R (Figure 2). Therefore, the impossibility of incorporating T2F in microtubules is most likely due to the stabilization of the complex with its 3D curvature which does not allow lateral interactions to be established as occurs in growing microtubules. Consistent with this conclusion, a 102-residue region (residues 40 to 141) of stathmin inhibited microtubule polymerization but not formation of the tubulin double rings which are obtained at high magnesium concentration and have a curvature similar to that of T2R (Steinmetz et al., 2000). When presented with the right curvature of a tubulin assembly, this stathmin region does not prevent tubulin polymerization.

Two mechanisms by which stathmin regulates tubulin assembly have been advocated, catastrophe promotion (Belmont and Mitchison, 1996; Howell et al., 1999) and tubulin sequestration (Curmi et al., 1997; Jourdain et al., 1997). The structure we determined gives a satisfactory explanation to the sequestering capacity of stathmin or of proteins of the stathmin family. To promote catastrophes it is expected that stathmin must interact with microtubule ends, either straight or curved. Taken together, the observations that stathmin binds to GTP-tubulin with lower affinity than to GDP-tubulin and that the curvature of GDP-tubulin oligomers is larger by a factor of two than that of tubulin oligomers bound to a slowly hydrolyzable analog of GTP (Müller-Reichert et al., 1998) show that the long helix of the RB3-SLD fits better the more curved GDP-tubulin oligomers. If we consider the hypothesis that stathmin may bind to the curved extremities of microtubules, it has been shown that stathmin, as opposed to its α-helical region, is unable to associate with similarly curved tubulin rings, suggesting a capping effect for the 40-residue N-terminal region (Steinmetz et al., 2000). This is consistent with our observation that the long RB3-SLD helix extends to the ends of T2R. It could therefore be possible that stathmin caps and stabilizes otherwise transient protofilament curls at the tips of microtubules. The relative efficiencies of the catastrophe promoting and sequestering activities of stathmin would then depend on the frequency of occurrence of these curls and on the relative affinities of stathmin for them and for soluble tubulin.

The Curved Structure of GDP-Tubulin

The curvature of T2R (in which GDP is the exchangeable nucleotide) is identical to that of the depolymerization products of GDP-microtubules (Müller-Reichert et al., 1998). This suggests that binding to the RB3-SLD does not significantly affect the shape of GDP-tubulin and that the structure of tubulin in T2R reflects the structures of GDP-tubulin oligomers and of GDP-tubulin in curved tubulin protofilaments. Comparison with the structure of straight tubulin in microtubules can therefore give clues as to the mechanism involved in the microtubule assembly–disassembly process. Indeed, although the present resolution of our model does not allow a description of how the curvature of T2R or GDP-tubulin oligomers is accommodated at the atomic level in tubulin subunits, it does provide an overall measure of the structural differences between soluble GDP-tubulin and straight microtubule tubulin. When the α tubulin subunit in microtubules and the α_1 subunit of T2R are superimposed (rmsd of Cαs: 1.7 Å), the rmsd between the Cα positions of the β and β_1 subunits is 5.8 Å. This structural difference may be attributed to changes in loop conformations and to two movements of β subunit domains. The first involves a rotation of 11° that superimposes the β subunit nucleotide binding domain on that of the β_1 subunit. A better fit is achieved when this movement is followed by a smaller rotation of the intermediate domain. The change of the relative orientations of the nucleotide binding domains of tubulin subunits with respect to the conformation locked in microtubules is the most significant component of the overall structural difference between tubulin in T2R and in straight protofilaments. It is accompanied by an increase in the distance and a lowering of the buried, interacting areas between subunits within the tubulin heterodimer and between heterodimers. These differences are required to account for the curvature of T2R (Figure 4). Such changes of the relative orientations of tubulins and tubulin subunits with respect to those in microtubules would also account for the curvature of GDP-tubulin oligomers and depolymerizing protofilaments. These differences provide direct evidence for different conformations of GDP-tubulin in curved oligomers and straight microtubules (Melki et al., 1989), the straightening of GDP-tubulin resulting probably from lateral interactions within the microtubule. It is therefore tempting to suggest that these differences of GDP-tubulin in oligomers and microtubules constitute at least part of the structural cause of the spring load that has been proposed (Caplow et al., 1994) to drive the rapid depolymerization associated with the dynamic instability of microtubules.

In conclusion, the present crystal structure of a tubulin:SLD complex allows us to picture the molecular organization of tubulin-GDP in solution and the functional interactions of stathmin and stathmin family proteins in a tubulin sequestering complex. Structural studies with other forms of both tubulin- and stathmin-related molecules will give further information required for a molecular description of the biological action of stathmin family molecules as well as of regulatory processes involved in the control of microtubule dynamics.

Experimental Procedures

Affinity Measurements

Sensor chips CM5, HBS buffer and amine coupling kit containing N-hydroxysuccinimide (NHS), N-ethyl-N'-(3-diethyl-aminopropyl)-carbodiimide (EDC) and 1 M ethanolamine-hydrochloride pH 8.5 were from Pharmacia Biosensor AB, (Uppsala, Sweden). Flowcells were prepared with stathmin or RB3-SLD. Immobilization of proteins to the CM5 sensor chip was performed in the Biacore system as described (Curmi et al., 1997). Buffer AB (80 mM K-Pipes pH 6.8, 1 mM EGTA, 1 mM $MgCl_2$) was used throughout this study. Interaction of GDP- or GTP-tubulin with immobilized stathmin or RB3-SLD was studied over a tubulin concentration range of 2–8 μM. An analytical cycle consisted in the injection of tubulin at increasing concentrations (2, 4, 8 μM) in AB buffer at a flow-rate of 10 μl/min at 25°C. Interaction curves were obtained and data evaluated for kinetic analysis as described (Curmi et al., 1997).

Purification, Crystallization, Data Collection and Processing

Bovine brain tubulin was purified by two cycles of polymerization and depolymerization followed by phosphocellulose chromatography (Mitchison and Kirschner, 1984). The product was stored at −80°C in 20 mM K-Pipes pH 6.8, 0.25 mM EGTA, 0.25 mM $MgCl_2$, until use. RB3-SLD, represents residues 49–189 of RB3 flanked by an additional alanine at its N terminus (amino acid residues are numbered from 2, residue 1 representing the N-terminal cleaved methionine encoded by the mRNA). RB3-SLD corresponds to stathmin residues 5 to 145 (local alignment between stathmin 5–145 and RB3-SLD shows a 72% identity with no gap). In the text, residue numbering of both stathmin and RB3-SLD is according to the stathmin sequence. The RB3-SLD cDNA was subcloned into the NcoI-BamHI sites of the expression vector pET-8c, which was then used to transform the BL21(DE3) *E. coli* strain. Recombinant RB3-SLD was expressed and purified to homogeneity as described for stathmin (Curmi et al., 1994). At the end of the purification process, pure RB3-SLD was desalted and concentrated in 1 mM DTT using a centriprep-10 (Amicon) and then stored at −80°C until use. All protein concentrations were determined by amino acid analysis.

GDP-Tubulin was mixed with RB3-SLD in a 2:1 tubulin:RB3-SLD molar ratio, and the complex at a concentration of 15 mg/ml was crystallized by the hanging drop method at pH 7.0 using Polyethylene Glycol as a precipitant. Crystals appeared in one or two days and they reached their maximal size ($300 \times 300 \times 800\ \mu m^3$) in no more than one week. Crystals most often crack when they are harvested but anneal over a period of a few minutes. For data collection, crystals were transferred in a stabilizing solution containing also 20% ethylene glycol as cryoprotectant and were flash-frozen in liquid ethane. A complete data set to 3.95 Å resolution was collected at 100 K on the ID14–2 beamline of the ESRF synchrotron (Grenoble, France). We used the HKL package (Otwinowsky and Minor, 1997) to process the data. Statistics are summarized in Table 1.

Structure Determination and Refinement

The crystal structure of T2R was determined by the Molecular Replacement method using the AMoRe package (Navaza, 1994). The search was done using the tubulin model determined by electron crystallography (PDB code 1TUB) (Nogales et al., 1998). The successful search used a model consisting of the Cα of the secondary structure elements of tubulin. There were two independent tubulins to be positioned. Rotation and translation functions were calculated over the 15–4.8 Å resolution range (16,320 reflections). All orientations from the rotation function were input to one-body fast translation function (Navaza and Vernoslova, 1995) after which the figure of merit chosen for evaluation was the correlation coefficient of observed and calculated structure factor amplitudes. In view of the overall dimensions of tubulin, a 35 Å cutoff distance of centers of mass of two symmetry-related tubulins was applied to eliminate overlapping positions. Fast rigid-body least-squares refinements of the 300 highest ranking positions of tubulin were performed at 7 Å resolution (4,913 reflections). At the end of this procedure, there was no contrast between the figures of merit of the various tubulin positions resulting from our calculations.

Contrast among the figures of merit of Molecular Replacement solutions after rigid body refinement is usually taken as a landmark of the success of the procedure. We reasoned that the absence of contrast in our Molecular Replacement calculations might be due to an incorrect conformation of tubulin. The 300 top ranking tubulin positions were therefore split into two subunits (α and β) and refined as two rigid bodies; thereafter a contrast was detected. The new conformation of tubulin, noted (α/β)′, corresponding to the top-ranking position (correlation coefficient of observed and calculated structure factor amplitudes: 41.6%), was used as a new search model for a 2-body phased translation function calculation. This approach led to a contrasted two-(α/β)′ bodies solution (correlation coefficient of calculated and observed structure factor amplitudes: 51.3%; next higher figure of merit: 41.8%) after two tubulin rigid body refinement. After four subunit rigid body refinement, this coefficient rose to 53.6%. The final molecular replacement model comprised all atoms of the tubulin electron crystallography structure.

After molecular replacement, the structure was refined by simulated annealing of torsion angle parameters as implemented in CNS (Rice and Brunger, 1994; Brunger et al., 1998), followed by grouped B factor refinement. During refinement, noncrystallographic symmetry constraints were initially applied to α and β subunits separately. Since the two tubulins turned out to have the same conformation, in all subsequent refinement cycles noncrystallographic restraints were applied to tubulins. A 91-residue helix was located in a synthesis map calculated after solvent flipping and truncation density modification (Abrahams and Leslie, 1996) and was attributed to RB3-SLD. Probably because of the high solvent content of the crystals, this map was of far better quality than that of weighed $2F_{obs} - F_{calc}$ maps. All maps were computed with the CNS package (Brunger et al., 1998) and visualized in O (Jones et al., 1991). The current model comprises the tubulin heterodimer except the C-terminal residues (441–Cter in the α subunit and 438–Cter in the β subunit) and the H1 –B2 loops, 91 residues of RB3-SLD modeled as a polyAla α helix, and one nucleotide in each tubulin subunit binding site (GTP in the α chain and GDP in the β chain, according to the content of the crystal). Statistics are summarized in Table 1. Coordinates have been deposited in the Protein Data Bank (code: 1FFX).

Acknowledgments

We gratefully acknowledge discussions with Dr. M.-F. Carlier, advice on Molecular Replacement from Dr. J. Navaza, and critical reading of this manuscript by Dr. J. Janin, Dr. R.-M. Mège, and Dr. J. J. Skehel. We thank Dr. E. Nogales for communicating microtubule coordinates. Beamtime at the ELETTRA synchrotron (Trieste) and on beamline ID14 of the ESRF synchrotron (Grenoble) is gratefully acknowledged. This work was supported by grants from C.N.R.S., I.N.S.E.R.M., A.R.C., and A.F.M.

Received May 30, 2000; revised July 13, 2000.

References

Abrahams, J.P., and Leslie, A.G.W. (1996). Methods used in the structure determination of bovine mitochondrial F1 ATPase. Acta Crystallogr. D *52*, 30–42.

Altschul, S.F., Madden, T.L., Schaffer, A.A., Zhang, J., Zhang, Z., Miller, W., and Lipman, D.J. (1997). Gapped BLAST and PSI-BLAST: a new generation of protein database search programs. Nucleic Acids Res. *25*, 3389–3402.

Antonsson, B., Kassel, D.B., Di Paolo, G., Lutjens, R., Riederer, B.M., and Grenningloh, G. (1998). Identification of in vitro phosphorylation sites in the growth cone protein SCG10. Effect of phosphorylation site mutants on microtubule-destabilizing activity. J. Biol. Chem. *273*, 8439–8446.

Belmont, L.D., and Mitchison, T.J. (1996). Identification of a protein that interacts with tubulin dimers and increases the catastrophe rate of microtubules. Cell *84*, 623–631.

Brunger, A.T., Adams, P.D., Clore, G.M., DeLano, W.L., Gros, P., Grosse-Kunstleve, R.W., Jiang, J.S., Kuszewski, J., Nilges, M., Pannu, N.S., et al. (1998). Crystallography & NMR system: a new software suite for macromolecular structure determination. Acta Crystallogr. D *54*, 905–921.

Caplow, M., Ruhlen, R.L., and Shanks, J. (1994). The free energy of hydrolysis of a microtubule-bound nucleoside triphosphate is near zero: all of the free energy for hydrolysis is stored in the microtubule lattice. J. Cell Biol. *127*, 779–788.

CCP4 (1994). The CCP4 suite: programs for protein crystallography. Acta Crystallogr. D *50*, 760–763.

Curmi, P., Maucuer, A., Asselin, S., Lecourtois, M., Chaffotte, A., Schmitter, J.M., and Sobel, A. (1994). Molecular characterization of human stathmin expressed in *Escherichia coli*: site-directed mutagenesis of two phosphorylatable serines (Ser-25 and Ser-63). Biochem. J. *300*, 331–338.

Curmi, P.A., Andersen, S.S.L., Lachkar, S., Gavet, O., Karsenti, E., Knossow, M., and Sobel, A. (1997). The stathmin tubulin interaction in vitro. J. Biol. Chem. *272*, 25029–25036.

Diaz, J.F., Pantos, E., Bordas, J., and Andreu, J.M. (1994). Solution

structure of GDP-tubulin double rings to 3 nm resolution and comparison with microtubules. J. Mol. Biol. *238*, 214–225.

Di Paolo, G., Antonsson, B., Kassel, D., Riederer, B.M., and Grenningloh, G. (1997). Phosphorylation regulates the microtubule-destabilizing activity of stathmin and its interaction with tubulin. FEBS Lett. *416*, 149–152.

Doye, V., Soubrier, F., Bauw, G., Boutterin, M.C., Beretta, L., Koppel, J., Vandekerckhove, J., and Sobel, A. (1989). A single cDNA encodes two isoforms of stathmin, a developmentally regulated neuron-enriched phosphoprotein. J. Biol. Chem. *264*, 12134–12137.

Esnouf, R.M. (1997). An extensively modified version of MolScript that includes greatly enhanced coloring capabilities. J. Mol. Graph. *15*, 133–138.

Gavet, O., Ozon, S., Manceau, V., Lawler, S., Curmi, P., and Sobel, A. (1998). The stathmin phosphoprotein family: intracellular localization and effects on the microtubule network. J. Cell Sci. *111*, 3333–3346.

Gradin, H.M., Larsson, N., Marklund, U., and Gullberg, M. (1998). Regulation of microtubule dynamics by extracellular signals: cAMP-dependent protein kinase switches off the activity of oncoprotein 18 in intact cells. J. Cell Biol. *140*, 131–141.

Hailat, N., Strahler, J.R., Melhem, R.F., Zhu, X.X., Brodeur, G., Seeger, R.C., Reynolds, C.P., and Hanash, S.M. (1990). N-myc gene amplification in neuroblastoma is associated with altered phosphorylation of a proliferation related polypeptide (Op 18). Oncogene *5*, 1615–1618.

Horwitz, S.B., Shen, H.J., He, L., Dittmar, P., Neef, R., Chen, J., and Schubart, U.K. (1997). The microtubule-destabilizing activity of metablastin (p19) is controlled by phosphorylation. J. Biol. Chem. *272*, 8129–8132.

Howell, B., Larsson, N., Gullberg, M., and Cassimeris, L. (1999). Dissociation of the tubulin-sequestering and microtubule catastrophe-promoting activities of oncoprotein 18/stathmin. Mol. Biol. Cell. *10*, 105–118.

Jones, T.A., Zhou, J.-Y., Cowan, S.W., and Kjeldgaard, M. (1991). Improved methods for building protein models in electron density maps and the location of errors in these models. Acta Crystallogr. *A47*, 110–119.

Jourdain, L., Curmi, P., Sobel, A., Pantaloni, D., and Carlier, M.-F. (1997). Stathmin is a tubulin sequestering protein which forms a ternary T2S complex with two tubulin molecules. Biochemistry *36*, 10817–10821.

Kraulis, P. (1991). MOLSCRIPT: a program to produce both detailed and schematic plots of protein structures. J. Appl. Crystallogr. *24*, 924–950.

Larsson, N., Segerman, B., Melander Gradin, H., Wandzioch, E., Cassimeris, L., and Gullberg, M. (1999). Mutations of oncoprotein 18/stathmin identify tubulin-directed regulatory activities distinct from tubulin association. Mol. Cell. Biol. *19*, 2242–2250.

Mandelkow, E.M., Mandelkow, E., and Milligan, R.A. (1991). Microtubule dynamics and microtubule caps: a time-resolved cryo-electron microscopy study. J. Cell Biol. *114*, 977–991.

Marklund, U., Larsson, N., Brattsand, G., Osterman, O., Chatila, T.A., and Gullberg, M. (1996). Oncoprotein 18 is a phosphorylation-responsive regulator of microtubule dynamics. EMBO J. *15*, 5290–5298.

Maucuer, A., Doye, V., and Sobel, A. (1990). A single amino acid difference distinguishes the human and the rat sequences of stathmin, a ubiquitous intracellular phosphoprotein associated with cell regulations. FEBS Lett. *264*, 275–278.

Maucuer, A., Moreau, J., Mechali, M., and Sobel, A. (1993). The stathmin gene family: phylogenetic conservation and developmental regulation in Xenopus. J. Biol. Chem. *268*, 16420–16429.

Melander Gradin, H., Marklund, U., Larsson, N., Chatila, T.A., and Gullberg, M. (1997). Regulation of microtubule dynamics by Ca2+/calmodulin-dependent kinase IV/Gr-dependent phosphorylation of oncoprotein 18. Mol. Cell. Biol. *17*, 3459–3467.

Melki, R., Carlier, M.F., Pantaloni, D., and Timasheff, S.N. (1989). Cold depolymerization of microtubules to double rings: geometric stabilization of assemblies. Biochemistry *28*, 9143–9152.

Mitchison, T.J., and Kirschner, M.W. (1984). Dynamic instability of microtubule growth. Nature *312*, 237–242.

Müller-Reichert, T., Chrétien, D., Severin, F., and Hyman, A.A. (1998). Structural changes at microtubule ends accompanying GTP hydrolysis: information from a slowly hydrolyzable analogue of GTP, guanylyl (α,β)methylenediphosphonate. Proc. Natl. Acad. Sci. USA *95*, 3661–3666.

Navaza, J. (1994). AMoRe: an automated package for molecular replacement. Acta Crystallogr. A *50*, 157–163.

Navaza, J., and Vernoslova, E. (1995). On the fast translation functions for molecular replacement. Acta Crystallogr. A *51*, 445–449.

Nogales, E., Wolf, S.G., and Downing, K.H. (1998). Structure of the $\alpha\beta$ tubulin dimer by electron crystallography. Nature *391*, 199–203.

Nogales, E., Whittaker, M., Milligan, R.A., and Downing, K.H. (1999). High-resolution model of the microtubule. Cell *96*, 79–88.

Otwinowsky, Z., and Minor, W. (1997). Processing of X-ray diffraction data collected in oscillation mode. Methods Enzymol. *276*, 307–325.

Ozon, S., Maucuer, A., and Sobel, A. (1997). The stathmin family—molecular and biological characterization of novel mammalian proteins expressed in the nervous system. Eur. J. Biochem. *248*, 794–806.

Redeker, V., Lachkar, S., Siavoshian, S., Charbaut, E., Rosier, J., Sobel, A., and Curmi, P.A. (2000). Probing the native structure of stathmin and its interaction domains with tubulin. J. Biol. Chem. *275*, 6841–6849.

Rice, L.M., and Brunger, A.T. (1994). Torsion angle dynamics: reduced variable conformational sampling enhances crystallographic structure refinement. Proteins: Struct. Funct. Genet. *19*, 277–290.

Riederer, B.M., Pellier, V., Antonsson, B., Di Paolo, G., Stimpson, S.A., Lutjens, R., Catsicas, S., and Grenningloh, G. (1997). Regulation of microtubule dynamics by the neuronal growth-associated protein SCG10. Proc. Natl. Acad. Sci. USA *94*, 741–745.

Rost, B., Sander, C., and Schneider, R. (1994). PHD—an automatic server for protein secondary structure prediction. CABIOS *10*, 53–60.

Sobel, A. (1991). Stathmin: a relay phosphoprotein for multiple signal transduction? Trends Biochem. Sci. *16*, 301–305.

Sobel, A., Boutterin, M.C., Beretta, L., Chneiweiss, H., Doye, V., and Peyro-Saint-Paul, H. (1989). Intracellular substrates for extracellular signaling: characterization of a ubiquitous, neuron-enriched phosphoprotein (stathmin). J. Biol. Chem. *264*, 3765–3772.

Steinmetz, M.O., Kammerer, R.A., Jahnke, W., Goldie, K.N., Lustig, A., and van Oostrum, J. (2000). Op18/stathmin caps a kinked protofilament-like tubulin tetramer. EMBO J. *19*, 572–580.

Wallon, G., Rappsilber, J., Mann, M., and Serrano, L. (2000). Model for stathmin/OP18 binding to tubulin. EMBO J. *19*, 213–222.

Protein Data Bank ID Code

The coordinates reported in this article have been deposited in the Protein Data Bank under ID code 1FFX.